Regular Article

PHYSICAL CHEMISTRY RESEARCH
Published by the
Iranian Chemical Society
www.physchemres.org
info@physchemres.org

Phys. Chem. Res., Vol. 12, No. 3, 663-674, September 2024
DOI: 10.22036/pcr.2023.416669.2419

First-Principles Investigation of Structural Stability, Electronic, and Optical Properties of V, Y-Doped, and (V, Y)-Codoped Monoclinic ZrO_2

F. Saidi[a,b,*], M. Dergal[a], A. Dendane[a] and N. Ameur[c]

[a]*Division of Materials Discovery (DEPM)-Unit of Research on Materials and Renewable Energies (URMER)-AbouBekrBelkaid University of Tlemcen (Algeria)*

[b]*High School in Electrical and Energetic Engineering ESGEE-Oran*

[c]*Laboratory of Catalysis and Synthesis in Organic Chemistry (LCSCO), University of Tlemcen, Imama, BP 119, 13000 Tlemcen, Algeria*

(Received 16 September 2023, Accepted 30 November 2023)

To enhance the electrical and optical properties of zirconium dioxide (ZrO_2) for industrial applications, we conducted a study investigating the influence of two transition metals on the characteristics of monoclinic ZrO_2. The investigation involved the use of the plane-wave ultrasoft pseudopotential technique, which relies on first-principles density-functional theory (DFT). Our comprehensive analysis covered various aspects, including the assessment of structural parameters, elastic behavior, electronic structure, bonding properties, and optical characteristics of monoclinic ZrO_2, along with its (V-Y)-doped and V, Y-codoped variations. Our estimations of the structural properties and independent elastic constants of monoclinic ZrO_2 aligned well with previous research findings. To examine the electronic structure and bonding characteristics, we utilized densities of states and charge densities. Notably, the analysis of optoelectronic properties revealed that the addition of V and Y dopants led to a significant reduction in the band gap of ZrO_2. This phenomenon is attributed to the appearance of impurity states linked to V and Y in the valence band's spin. Moreover, the incorporation of V and Y separately or together into ZrO_2 resulted in a remarkable increase in the refractive index and the generation of distinct absorption peaks within the visible range, presenting exciting possibilities for potential applications in photo absorption.

Keywords: ZrO_2, Electronic properties, Optical properties, First-principles, Substitution, Doping, VY-ZrO_2

INTRODUCTION

Zirconium dioxide (ZrO_2) is a valuable material widely utilized in modern industrial applications, such as heterogeneous catalysts, solid oxide cells, semiconductors, and optoelectronic devices [1-2]. Recently, several experimental techniques, including spark plasma sintering (SPS) [3], hot quasi-static compaction [4], and laser-engineered net shaping [5] have been employed to produce bulk or coated ZrO_2.

Due to its excellent dielectric characteristics, broadband gap, and high melting point [6], ZrO_2 has been the subject of extensive experimental and theoretical research. Additionally, ZrO_2 exhibits one of the highest dielectric constants, making it a promising candidate for protective and optical coatings. The electrical structures and optical characteristics of thermally annealed ZrO_2 samples are determined by the precise preparation method and resulting structural parameters [7,8].

Under atmospheric pressure, ZrO_2 can exist in three polymorphs: monoclinic (m-ZrO_2), tetragonal (t-ZrO_2), and cubic fluorite (c-ZrO_2) phases. Unlike tetragonal and cubic zirconia crystals, which are unstable at ambient temperature, monoclinic zirconia remains stable even at temperatures beyond 1170 °C [9,10]. The observed band gap of bulk ZrO_2 is 4.59 eV [11], rendering it suitable for applications in nanoelectronic materials and energy storage [12].

With its favorable refractive index and transparency,

*Corresponding author. E-mail: saidifatiha11@gmail.com

ZrO_2 is a highly esteemed optical material used in antireflection coatings, ophthalmic lenses, optical sensors, and LED technology [13,14]. It can be employed as a supplementary material, acting as a charge separator and light reflector, to address the limitations of titanium dioxide (TiO_2) in photoelectrodes for dye-sensitized solar cells (DSSCs), which include transparency and charge recombination at the interface. Furthermore, ZrO_2 can function as a light-absorbing layer in solar cells [15].

Recent research has revealed that undoped ZrO_2 exhibits d0 ferromagnetism, an unexpected phenomenon successfully reported by Venkatesan *et al.* [16], opening up potential applications in spintronics. The characteristics and crystal structures of cubic ZrO_2 doped with transition metals have been investigated experimentally and theoretically by numerous research groups [17]. Additionally, there has been significant interest in the possibility of inducing ferromagnetism in ZrO_2 and TiO_2 through carbon doping [18].

Considerable research [19,20] has been devoted to investigating the potential ferromagnetism induced by transition metal doping in semiconductor oxides like ZrO_2. Diluted magnetic semiconductors (DMSs) [21] have particularly demonstrated remarkable performance in this field, owing to the significant impact of ferromagnetism in semiconductor metal oxides on spintronic and optoelectronic applications. However, it remains unclear whether ferromagnetism is an intrinsic characteristic of the system or arises from the interaction of magnetic impurities [22]. More recently, the anticipation of ferromagnetic behavior has also extended to oxides like ZrO2 doped with light 2p elements like nitrogen (N) [23]. Nevertheless, there is still ongoing debate regarding the cause of the magnetic behavior in such materials.

To overcome these limitations, alloying has proven to be a successful method for enhancing various properties of solid materials [24]. For example, Wang and Lin found that Cr doping improves the electrical and mechanical characteristics of cubic ZrO_2 [25]. Chouhan and Srivastava et al. reported that Ag doping enhances the ferromagnetic behavior of monoclinic ZrO2 [26]. Zhang and Han discovered that rare earth metals, such as Ce, La, Sm, and Y, greatly enhance the catalytic characteristics of ZrO2 [27]. Additionally, carbon (C) doping has garnered considerable interest as a potential technique for inducing ferromagnetism in ZrO_2 and TiO_2 [28].

H. Fayyaz *et al.* recently used density functional theory (DFT) to examine the electrical characteristics of doped ZrO_2, both with and without single oxygen vacancies (Vo) [23]. Among the numerous dopants, transition metals such as yttrium (Y) and vanadium (V) are preferred options due to their favorable physical and chemical properties [29-31]. Based on our findings, these transition metals may enhance the chemical and physical characteristics of solid materials. However, little is known about how transition metals affect the electrical and optical properties of monoclinic ZrO_2. Therefore, in this study, we employ first-principles simulations to investigate the effects of transition metals on the electrical and optical characteristics of monoclinic ZrO_2 [32]. The electronic structure study reveals the electrical and optical properties of V- and Y-doped, as well as co-doped, monoclinic ZrO_2. The results demonstrate that the addition of V and Y metals enhances the electrical properties of monoclinic ZrO_2, primarily due to the involvement of noble metal d states. Moreover, these transition metals cause significant changes in the optical absorbance of monoclinic ZrO_2, which is of considerable importance.

COMPUTATIONAL METHODS

To conduct the computational simulations, the Vienna ab initio simulation package (VASP) based on density functional theory (DFT) was utilized [33,34]. The electron-ion core interaction was characterized using projector augmented wave (PAW) potentials, known for producing more accurate results than ultra-soft pseudopotentials [35]. To account for exchange-correlation effects, various approximations were used in this study. Initially, the generalized gradient approximation Perdew-Burke-Ernzerhof (GGA-PBE) [36] was employed as it effectively represents the essential characteristics of the electronic structure. This approximation was utilized for the full relaxation of the structure, but it is known to underestimate band gap values. To overcome this limitation, the (GGA+U) approximation was introduced, with the U parameter set to 10 for d-Zr states, which corrects the band gap miscalculation of GGA-PBE. For the calculation of electrical structure and optical characteristics, the metaGGA: mBj approach was

used. Additionally, to reliably predict attributes above the band gap value, the modified Becke Johnson potential, or TB-mBJ [37], was employed. Previous studies on ZrO_2 have shown that this potential yields results that closely match experimental values, making it suitable for predicting and confirming the structural, electrical, and optical properties of ZrO_2 using this method.

For the pseudopotentials, the valence electron configurations used were [Kr] $5s^4d^5p$ for zirconium and [He] $2s^2p$ for oxygen, with corresponding core radii of 1.625 and 0.820. The basis sets were plane waves with a cutoff energy of 450 eV, and an energy convergence threshold of 10-6 eV was chosen. Convergence was achieved using a 6x6x6 mesh with Monkhorst-Pack grids optimized for the number of special "k" points in the first Brillouin zone (FBZ) mesh. In investigating the effects of doping and co-doping with V and Y, the GGA-PBE functional was applied to calculate the $Zr_{1-x}V_xO_2$, $Zr_{1-y}Y_yO_2$, and $Zr_{1-x-y}V_xY_yO_2$ systems. The reliability of these functional for novel systems and features can often be predicted. To achieve a 3% doping concentration, the stoichiometries $Zr_{31}O_{64}V$, $Zr_{31}O_{64}Y$, and $Zr_{30}O_{64}V_Y$ were obtained using the supercell method. The pseudopotentials for V and Y utilized valence electron configurations of [Ar] $3d^4s^4p$ and [Kr] $4s^4p^4d^5s$, respectively, with corresponding core radii of 1.323 and 1.815. The cutoff energy was set at 450 eV, and the energy convergence threshold was maintained at 10^{-6} eV. For each of the three systems, a 4x4x4 grid was used for the sampling of the Brillouin zone. Figure 1 illustrates the unit cells of V- or Y-doped ZrO_2 and V and Y co-doped ZrO_2 considered in this investigation.

To further investigate the energy stability of ZrO_2 and its various doped and co-doped combinations with Y and V, we analyzed the formation enthalpies using the following equations:

$$\Delta E_{form}^{ZrO_2} = E_{tot}^{ZrO_2} - (E_{tot}^{Zr} + 2\mu_O) \quad (1)$$

$$\Delta E_{form}^{doped} = E_{tot}^{doped} - E_{tot}^{ZrO_2} + E_{tot}^{Zr} + E_{tot}^{M} \quad (2)$$

At 0 K temperature and 0 Pa pressure, the enthalpies and formation energies are identical, meaning $\Delta E_{form} = \Delta H_{form}$ [38]. Here, $E_{tot}^{ZrO_2}$ and E_{tot}^{doped} represent the total energies of pure Zirconium dioxide and the doped configurations, respectively. $E_{tot}^{ZrO_2}$ is the energy per Zr atom in their solid state. μ_O is the chemical potential of oxygen, determined by the energy of the O_2 molecule ($\mu_O = \mu_O/2$). E_{tot}^{M} is the energy per Y or V atom in its most stable structure. For the calculation of the total energy, the relative elements are taken as listed in Table 1.

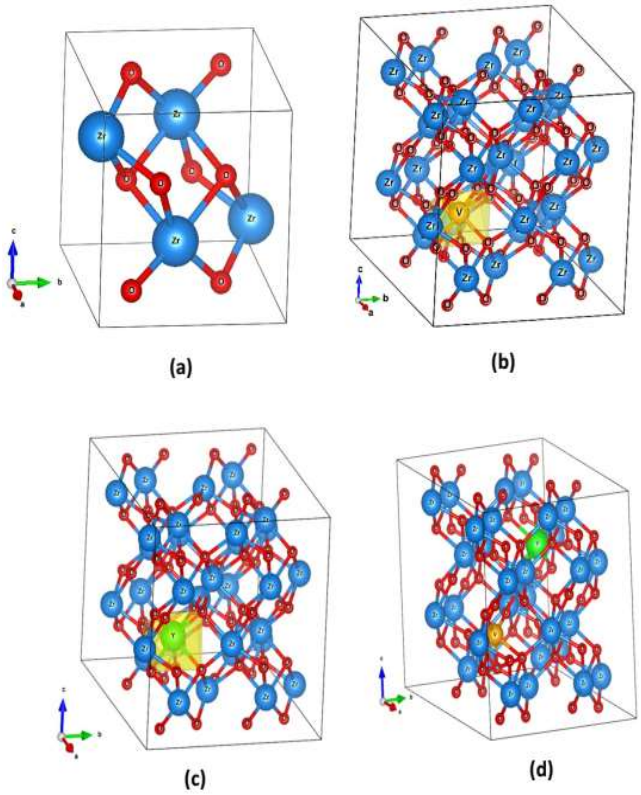

Fig. 1. Schematic representation of pure Zirconium dioxide ZrO_2 (a) and supercells of (b) V-doped, (c) Y-doped, and (d) V, Y-codoped monoclinic ZrO_2.

Table 1. Enthalpy of Formation (ΔH form in eV/atom) for both Pure and Doped Compounds

Système	ΔH_{form} (eV)
V-ZrO_2	-0,0028
Y-ZrO_2	-0,045
VY-ZrO_2:	-0,051

RESULTS AND DISCUSSION

Structural Properties

The monoclinic structure of pure ZrO_2 (m-ZrO_2) belongs to the space group P21/c (N° 14). To accurately describe the equilibrium properties of monoclinic ZrO_2, we analyzed the total energy for several lattice values. For computational efficiency, we utilized the VASP code to perform the calculations. By varying the volume, we determined the equilibrium lattice parameters and bulk modulus. The E *vs*. V curves were fitted using the Murnaghan equation of state [39].

To investigate the structural characteristics of stable ZrO_2, we adjusted the lattice parameters generated by GGA-PBE. Figure 2 illustrates the variations in total energy concerning the ratios of lattice parameters (b/a), (c/a), and volume. This analysis allowed us to identify the equilibrium structural parameters and gain insights into the energy landscape of ZrO_2.

By interpolating the data from Figure 2, we calculated the compression modulus B, its derivative B', the equilibrium volume, and the energy of the ground state. The outcomes are summarized in Table 2. The compression modulus B_0 (in GPa), lattice parameters a (in Å), b/a, c/a, and other theoretical and experimental research findings are shown to be consistent [25,37].

Electronic Properties

To analyze the behavior of pure zirconium dioxide (ZrO_2), we have plotted the total and partial density of states

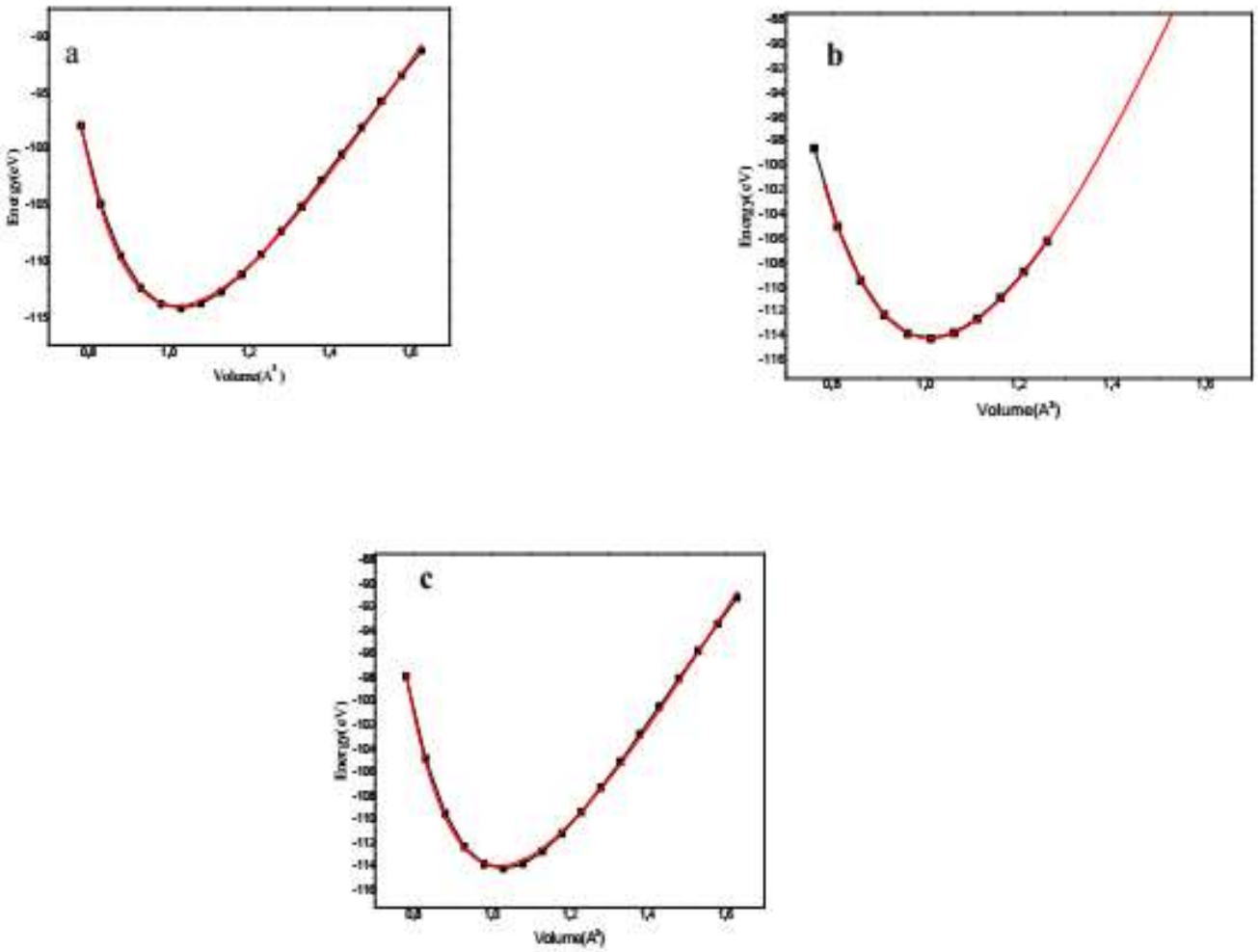

Fig. 2. Total energy of perfect monoclinic ZrO_2 as a function of the lattice parameter a (Å).

Table 2. Optimized Lattice Constants (a,b, and c in Å Unit) and Bulk Modulus (B in GPa), of Pure ZrO_2

Material	a (Å)	b/a	c/a	V (Å^3)	B_0(GPa)	B_0'
ZrO_2	5,208	1,011	1,030	145,27	241,2	4,3
	5,150[a]	1,011 [a]	1,032 [a]	142,72[a]	-	-
	5,197[b]	1,019 [b]	1,029 [b]	147,31[b]	-	-

[a]Ref. [39]. [b]Ref. [29].

(DOSs) as shown in Fig. 3. The calculated band gap energy of ZrO_2 is 3.6 eV, which is lower than the measured value of 5.8 eV presented in the figures. It is widely known that the PBE functional underestimates band gaps. To address this issue, we employed two additional approximations, GGA+U, and mBj, which aim to improve the description of the ground state of coupled systems. By increasing the Hubbard term's value to 5.1 eV in GGA+U to account for high screened intra-site Coulomb interactions among the 4d electrons of Zr, we were able to match the experimental band gap value. Similarly, mBj offered a gap adjustment of approximately 5.21 eV. Both GGA+U and mBj increased the band gap and introduced a new conduction band by shifting the conduction band's minimum to a higher energy.

Zirconium (Zr) and oxygen (O) have significantly different electronegativity values, 1.33 for Zr and 3.44 for O. The difference between these values (2.11) is higher than the reported value of 1.7 on the Pauling scale, indicating the presence of ionic bonds in the molecule. This idea is further supported by the partial DOS in Fig. 3, where the '4d' orbitals of Zr dominate above the Fermi level, and the '2p' orbitals of O dominate below. The 'up' and 'down' density of states (DOSs) are perfectly symmetrical, indicating that the material does not exhibit any magnetic activity.

Furthermore, in Fig. 4a, we show the total and projected density of states (DOS and PDOS) of the ZrO_2:V, ZrO_2:Y, and ZrO_2:VY systems in comparison to pure ZrO2. The ZrO_2:V system exhibits semiconductor behavior, which aligns with earlier theoretical predictions such as the 3.08 eV value calculated with the VASP program [40]. For the monoclinic phase, the band gap ranges between 3.4 and 5.4 eV when using the (SIESTA) package [41].

The addition of the V atom in ZrO_2 causes changes in the density of states. By replacing 4 Zr atoms, V contributes 5 valence electrons, leading to partial occupation of V's 3d

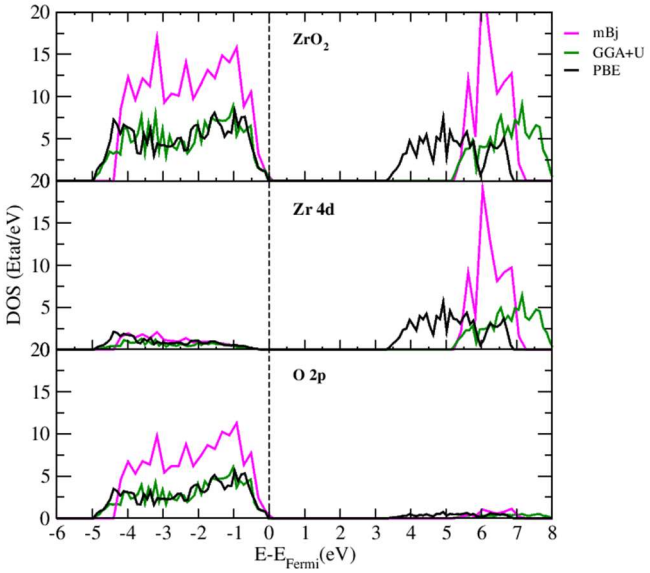

Fig. 3. Total density of states (DOS) for pure monoclinic ZrO_2 estimated using GGA-PBE, GGA+U, and mBj methods. The Fermi level (EF) is indicated by the vertical dashed line at E = 0 eV.

states, as depicted in Fig. 4b. Due to the low V concentration (3%), no isolated states appear in the band gap. The non-magnetic properties of doped ZrO_2 are further confirmed by the exact symmetry between spin-up and spin-down states. Compared to pure ZrO_2 (with a band gap of 3.6 eV), the addition of V shifts the valence and conduction bands apart, with the Fermi level moving closer to the band gap's center. In the case of the ZrO_2:Y system, the addition of the Y atom (providing 3 electrons to replace 4 Zr atoms) causes the valence band's maximum to move closer to the Fermi level. Similar to the band gap, no isolated states are present due to the low Y concentration (3%). Figure 4 shows that all of Y's 4d states are unoccupied.

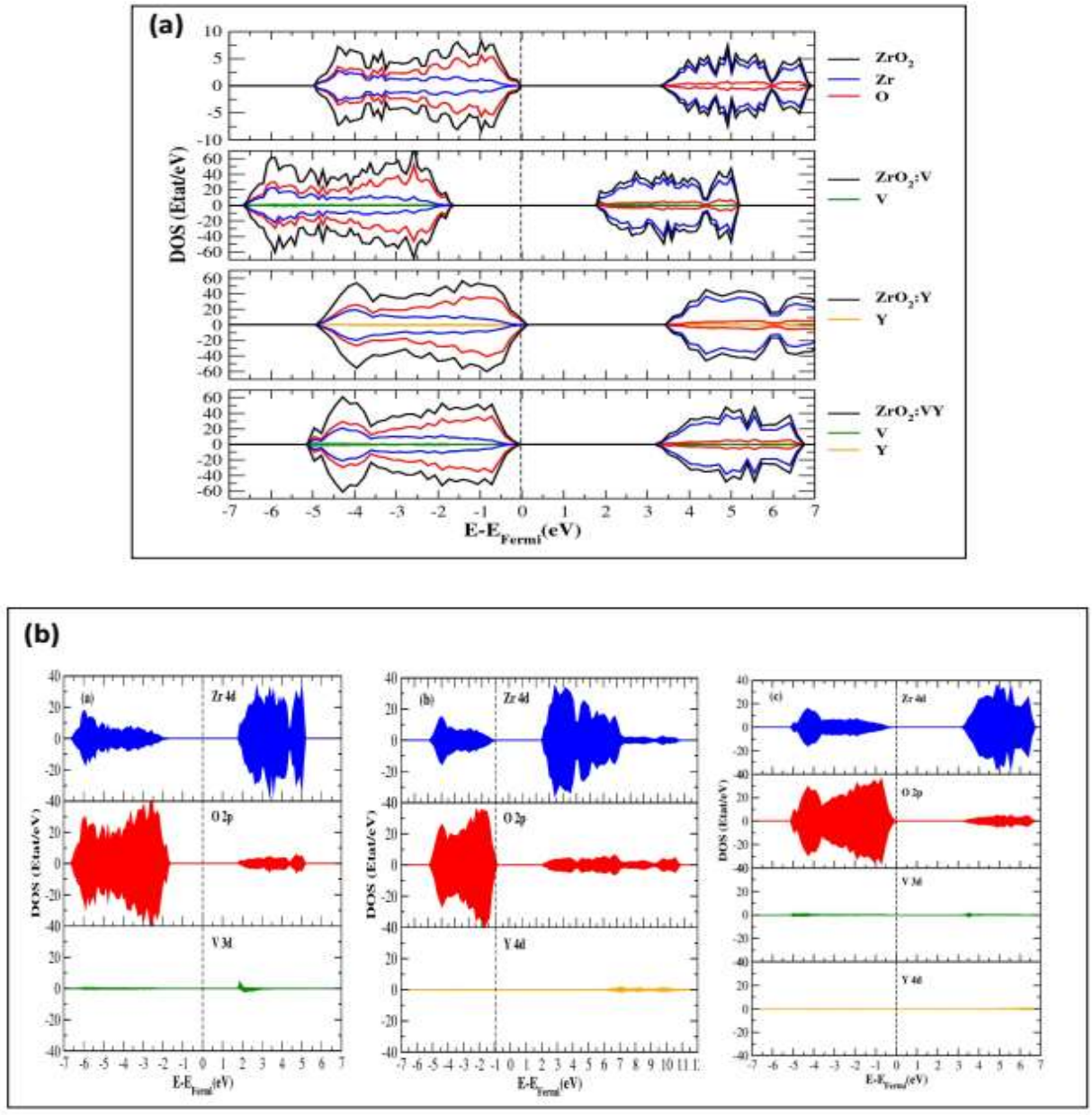

Fig. 4. Total density of states (DOS) for V, Y-doped, and (V, Y) codoped monoclinic ZrO_2 calculated using the GGA-PBE approach. The dashed vertical line at E = 0 eV represents the Fermi level (EF).

The ZrO_2:VY system is a p-type semiconductor, as evidenced by the total and projected density of states in Figs. 4a and b. The band gap value decreases compared to pure ZrO_2. The states close to the Fermi level are attributed to O 2p states with hybridization to Zr 4d states. The addition of V and Y atoms significantly shifts the valence band maximum away from the Fermi level, compared to the ZrO_2:Y system.

Table 3. Energy Gaps Obtained through the Application of Three Different Approximations: PBE, GGA+U, and mBj.

	PBE	GGA+U	mBj	Expérimental[a]
E_{gap} (eV)	3,6	5,1	5,21	5,6

[a]Ref. [21].

Experimental studies have also shown that the band gap decreases from 3.38 eV to 2.46 eV when Zr-V and Zr-Y bonds form [42-43]. The exact symmetry between the up and down densities of states confirms the absence of any magnetic behavior in this material.

To gain insights into the nature of chemical bonding, we provide the total charge densities and orbital bonding charge densities in the (110) plane, as shown in Fig. 5.

The bonding between Zr and O, as well as between V and O, largely exhibits a covalent nature due to the hybridization of Zr 4d and O 2p states. Additionally, we observe hybridization of Y 4d and O 2p orbitals, as well as V 3d and O 2p orbitals, indicating covalent interactions with some degree of ionic character. This phenomenon is influenced by the unique electronegativity characteristics of each atom, as reflected in the charge distribution. Our analysis of the state density supports these conclusions.

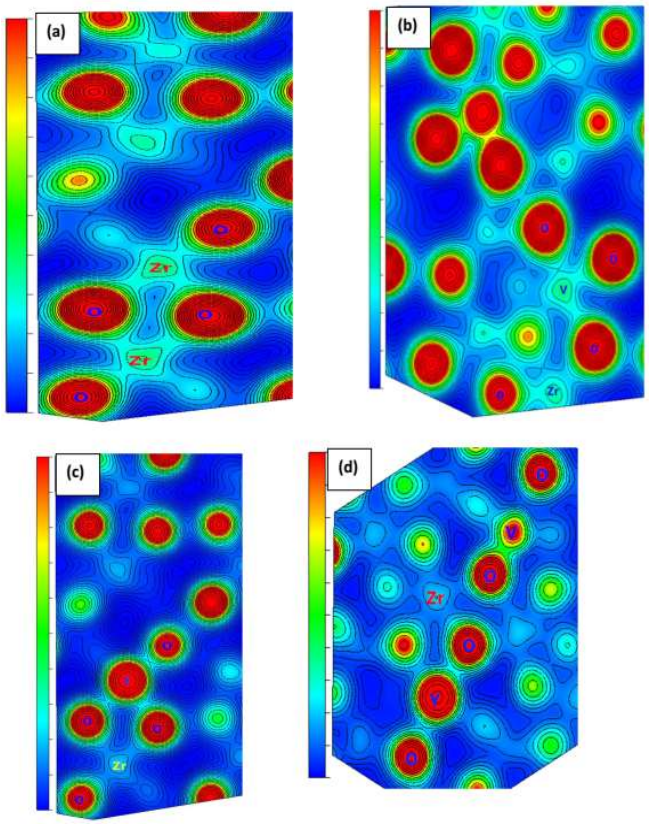

Fig. 5. Total charge density map of the (110) plane for (a) pure monoclinic ZrO_2, (b) V-doped ZrO_2, (c) Y-doped ZrO_2, and (d) V, Y-codoped ZrO_2.

Optical Properties

The optical characteristics of monoclinic ZrO_2 are then thoroughly investigated in relation to transition metals. The suitability of a material for use in optoelectronic devices is best determined by its optical properties. To evaluate all optical properties, the complex dielectric function $\varepsilon(\omega) = \varepsilon_1(\omega) + i\varepsilon_2(\omega)$ in the linear response range is used. The real portion of the dielectric constant, $\varepsilon_1(\omega)$, is determined using the well-known Kramers-Kronig relations [44,45] as follows:

$$\varepsilon_1(\omega) = 1 + \frac{2}{\pi} P \int_0^{\infty} \frac{\omega' \varepsilon_{2(\omega)}}{\omega'^2 - \omega^2 - i\eta} \tag{3}$$

The imaginary portion $\varepsilon_2(\omega)$ of the dielectric constant is computed by subtracting the occupied and unoccupied states from the momentum matrix elements.

$$\varepsilon_2(\omega) = \frac{4\pi^2 e^2}{\Omega} \lim_q \frac{1}{q^2} \sum_{c,v,k} 2w_k \delta(\varepsilon_{ck} - \varepsilon_{vk} - \omega) < u_{ck+e1q} | u_{vk} >< u_{ck+e2q} | u_{vk} > \tag{4}$$

where v and c are the coefficients determining the valence and conduction band states respectively. ε_{ck} and ε_{vk} are the energy levels. u_{ck+e1q} and u_{ck+e2q} are described as the cell's periodic phase of orbitals at the k-point. e and Ω indicate the elementary charge and the volume of the primitive cell, respectively. e1 and e2 are the unit vector's members.

The source of electron transition in substances can be estimated from the absorption coefficient $\alpha(\omega)$ which could also be computed using the following formula directly from the dielectric function:

$$\alpha(\omega) = \sqrt{2}\left(\frac{\omega}{c}\right)\left[\sqrt{\varepsilon_1^2(\omega) - \varepsilon_2^2(\omega)} - \varepsilon_1^2(\omega)\right] \tag{5}$$

The process of light absorption is commonly described as the substance absorbing photon energy through its electrons. Reflectivity of a surface measures the amount of radiation that is reflected back. Reflectivity is a specific case of reflectance used primarily to determine the incident and reflected light.

In this context, both reflection and absorption are essential optical factors to consider. Using the GGA, GGA+U, and GGA_ mBj approximations, Figs. 6 and 7

illustrate the optical spectra peaks of (Y-V)-doped and co-doped monoclinic ZrO_2, compared to pure ZrO_2. The optical absorption coefficient and reflectivity spectra for all compounds are shown for wavelengths between 100 and 900 nm. Photon absorption is a general term referring to the process of photon energy being absorbed by a substance through its electrons. Reflectivity, on the other hand, describes the radiation that a material reflects. The amount of incident and reflected light is often calculated using a specific type of reflectance. The main absorption peak of monoclinic ZrO_2 has been estimated to have an absorption coefficient of 175 nm, which aligns well with the findings of Sarhyaseelan, Maji, and Pan [46,47].

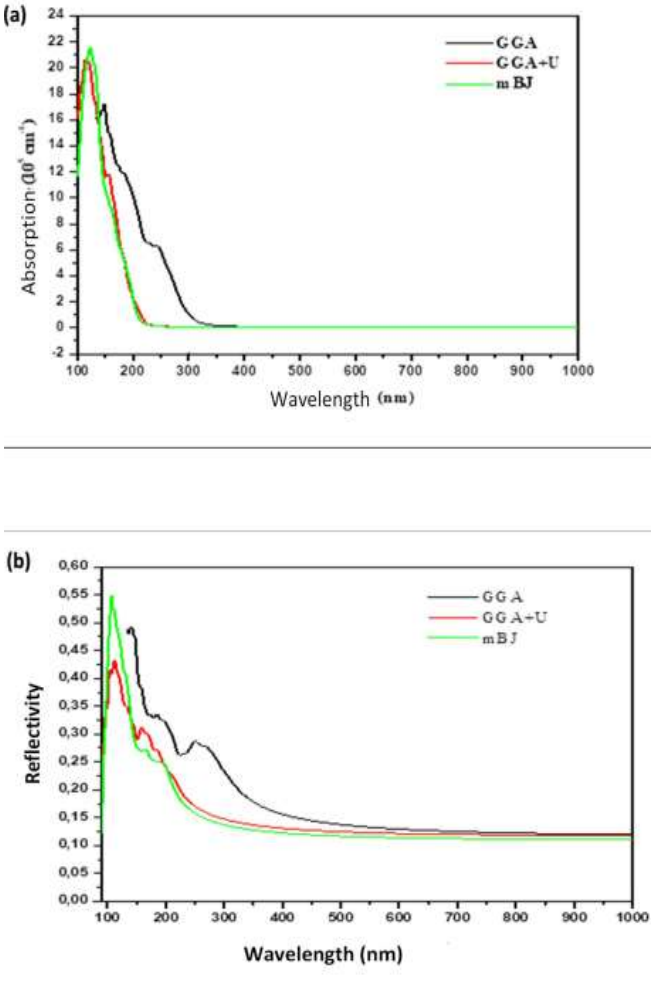

Fig. 6. Optical properties of pure ZrO_2: (a) Absorption coefficient and (b) Reflectivity, calculated using GGA-PBE, GGA+U, and mBj approaches.

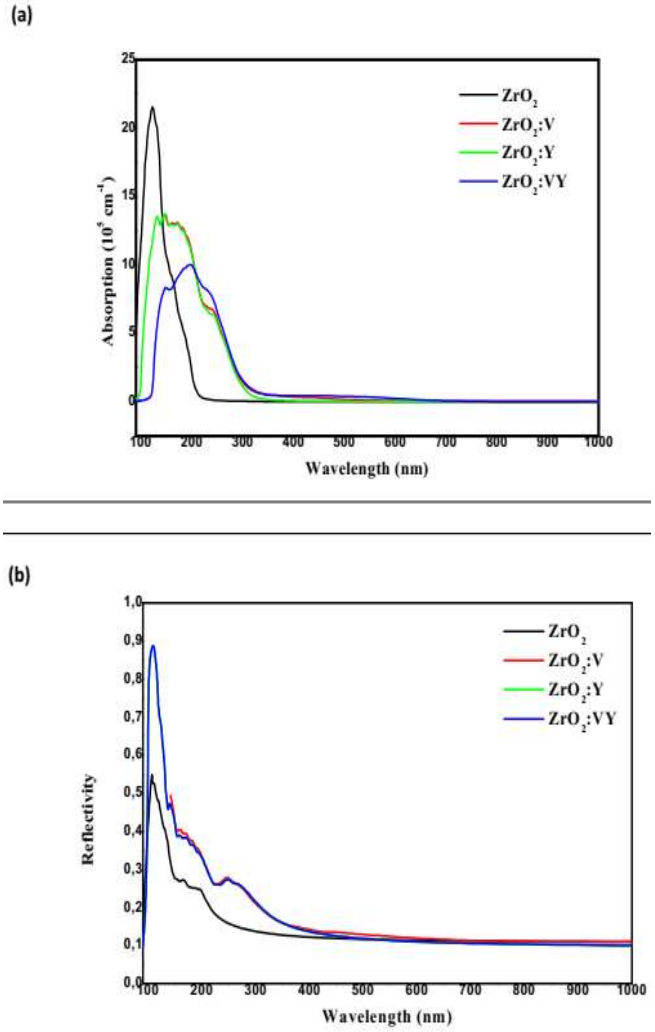

Fig. 7. Optical (a) absorption and (b) Reflectivity spectra of V-doped, Y-doped, and V, Y-codoped ZrO_2 compared to the pure case.

The spectra obtained using the three approximations, GGA, GGA+U, and GGA_mBj, exhibit minor differences. Notably, the absorption spectra show no significant absorption in the visible region between 380 nm and 750 nm, indicating that ZrO_2 is a good absorber in the ultraviolet (UV) range below 380 nm. This observation aligns well with experimental findings [37,55]. The absorption rates slightly vary among the three estimates, with GGA_mBj showing particularly strong absorption. The substance is transparent in the infrared region (above 750 nm), as evidenced by the very weak absorption observed.

The estimated density of states (DOS) indicates that the adsorption coefficient of perfect monoclinic ZrO2 is associated with the electronic transition between the occupied state of the valence band and the empty state of the conduction band. In the case of (V-Y)-doped ZrO_2, replacing one Zr atom with transition metals (V, Y) results in shifted optical adsorption, even though the value of the first major peak decreases compared to pure monoclinic ZrO_2. As shown in Fig. 7a, the absorption edges of (V-Y)-doped ZrO_2 extend to 400 nm for V and Y-doped ZrO_2 and 600 nm for V-Y-codoped ZrO_2. The introduction of transition metal d-states in monoclinic ZrO_2 doped with (V-Y) or co-doped with (Y and V) leads to enhanced light absorption in the visible spectrum compared to pure ZrO_2. The density of state (DOS) profiles (see Figs. 3 and 4) indicates that the presence of transition metal d-states is reflected by the V-O and Y-O bonds.

The reflectivity plots shown in Figs. 7a and b provide important insights into how light interacts with various materials. These plots reveal intriguing refractive behavior across different regions of the electromagnetic spectrum. For ZrO_2 and V, V-doped monoclinic ZrO_2, refractivity significantly influences their optical appearance. Notably, these materials display their highest reflectivity in the UV portion of the spectrum, indicating the absence of a band-gap energy at the Fermi level in this range. This suggests that ZrO_2 and V, V-doped monoclinic ZrO_2 readily reflect and absorb UV radiation. In the infrared domain, reflectance rapidly diminishes, indicating low infrared reflectivity and the potential for effective infrared radiation absorption. It is interesting to observe a drop in reflectivity in the ultraviolet region, particularly at around 300 nm, suggesting excellent transmittance and low reflection in the UV region below 300 nm for ZrO_2 and V, V-doped monoclinic ZrO_2. Analyzing the refractive behavior and reflectivity plots provides valuable insights into the optical properties of these materials, which are essential for various applications, including optoelectronics, sensors, and coatings, where the interaction of light with these materials plays a crucial role.

Figure 7a illustrates that pure ZrO_2 displays a strong absorption peak, which diminishes with V and Y doping. Moreover, there is a slight shift in the spectrum of doped ZrO_2 compared to the pure form, indicating that doping leads to a reduction in UV absorbance. The peak of ZrO_2 shifts lower with V doping and higher with Y doping, while reflectivity increases in this region. Furthermore, reflectivity remains at zero in the infrared band after V and Y doping.

Figures 6 and 7 clearly demonstrate that co-doping with V and Y significantly reduces absorbance and increases reflectivity in the ultraviolet range (below 380 nm). The peak obtained through co-doping is much smaller than that obtained through individual doping and pure ZrO_2. In the visible range, co-doping with vanadium and yttrium leads to a modest increase in reflectance, with similar trends observed in the UV spectrum.

CONCLUSION

In conclusion, our first-principles calculations have provided valuable insights into the impact of vanadium and yttrium transition metals on the electrical and optical characteristics of monoclinic ZrO_2. Analyzing the electronic structure of V, Y-doped, and co-doped ZrO_2 has revealed significant electronic and optical properties. The selection of V and Y as the transition metals was based on their elemental characteristics. To validate our results, we compared the structural details of the unit cell of monoclinic ZrO_2 with other experimental data.

The findings demonstrate that utilizing the MBj approximation, the computed band gap of ideal monoclinic ZrO_2 is 5.21 eV, showing good agreement with other theoretical findings. The band separation between the Fermi level and Zr-4d state and O-2p state, as revealed by the computed electronic structure, is responsible for the semiconductor characteristics of ZrO_2. For V-doped, Y-doped, and V-Y-codoped ZrO_2, the predicted band gaps are 3.65 eV, 3.5 eV, and 3 eV, respectively. This indicates that the addition of transition metals V and Y facilitates the electrical transition between the valence and conduction bands near the Fermi level. Moreover, the predicted adsorption peak of monoclinic ZrO_2 occurs at 178 nm.

The analysis of the energy loss function shows that the inclusion of Y and V metals leads to light-shifted optical adsorption in monoclinic ZrO_2. As mentioned earlier, we believe that these two metals not only enhance the optical properties but also improve the electrical properties of monoclinic ZrO_2. Overall, the presence of V and Y contributes to the enhancement of both the optical and electrical characteristics of monoclinic ZrO_2.

REFERENCES

[1] Chen, B.; Feng, T.; Chang, C.; Huang, S.; Jiang, B.; Shen, Z.; Kaichen Q.; Zhang, L., JO study of Nd-doped 8Y-ZrO_2 transparent ceramic and its potential application in infrared laser. *J. Alloys Compd.* **2021**, *884*, 161104. DOI: 10.1016/j.jallcom.2021.161104.

[2] Srichumpong, T.; Angkulpipat, S.; Prasertwong, S.; Thongpun, N.; Teanchai, C.; Veronesi, P.; Suputtamongkol K.; Leonelli C.; Heness G.; Chaysuwan, D., Effect of the crystallisation time and metal oxide pigments on translucency and the mechanical and physical properties of mica glass-ceramics. *J. Non-Cryst. Solids* **2020**, *528*, 119730. DOI: 10.1016/j.jnoncrysol.2019.119730.

[3] Li, J.; Meng, S.; Niu, J.; Lu, H., Electronic structures and optical properties of monoclinic ZrO_2 studied by first-principles local density approximation + U approach. *J. Adv. Ceram.* **2017**, *6*, 43-49. DOI: 10.1007/s40145-016-0216-y.

[4] Sayan, S.; Nguyen, N. V.; Ehrstein, J.; Emge, T.; Garfunkel, E.; Croft, M.; Zhao X.; Vanderbilt D.; Levin I.; Gusev E. P.; Hyoungsub K.; McIntyre, P. J., Structural, electronic, and dielectric properties of ultrathin zirconia films on silicon. *Appl. Phys. Lett.* **2005**, *86* (15). DOI: 10.1063/1.1864235.

[5] Garcia, J. C.; Scolfaro, L. M. R.; Lino, A. T.; Freire, V. N.; Farias, G. A.; Silva, C. C Leite Alves, H. W.; Rodrigues S. C. P.; Da Silva, E. F., Structural, electronic, and optical properties of ZrO_2 from ab initio calculations. *J. Appl. Phys.* **2006**, *100*(10). DOI:10.1063/1.2386967.

[6] Venkatesan, M.; Fitzgerald, C. B.; Coey, A. J., Unexpected magnetism in a dielectric oxide. *Nature* **2004**, *430* (7000), 630-630. DOI: 10.1038/430630a.

[7] Li, J.; Subramanian, M. A., Inorganic pigments with transition metal chromophores at trigonal bipyramidal coordination: Y (In, Mn) O_3 blues and beyond. *J. Solid State Chem.* **2019**, *272*, 9-20. DOI: 10.1016/j.jssc.2019.01.019.

[8] Fan, Z.; Zhao, Y.; Tan, Q.; Mo, N.; Zhang, M. X.; Lu, M.; Huang, H., Nanostructured Al_2O_3-YAG-ZrO_2 ternary eutectic components prepared by laser engineered net shaping. *Acta Mater.* **2019**, *170*, 24-37, DOI: 10.1016/j.actamat.2019.03.020.

[9] Bowman, W. J.; Yang, J.; Yildiz, B., The role of doping and microstructure on hydrogen solubility in monoclinic ZrO_2: Experimental validations of simulated defect chemistry. *Acta Mater.* **2020**, *195*, 172-183. DOI: 10.1016/j.actamat.2020.04.020.

[10] Yao, N. Q.; Liu, Z. C.; Gu, G. R.; Wu, B. J., Structural, optical, and electrical properties of Cu-doped ZrO_2 films prepared by magnetron co-sputtering. *Chin. Phys. B* **2017**, *26* (10), 106801. DOI: 10.1088/1674-1056/26/10/106801/meta.

[11] Archer, T.; Pemmaraju, C. D.; Sanvito, S., Magnetic properties of ZrO_2-diluted magnetic semiconductors. *J. Magn. Magn. Mater.* **2007**, *316* (2), 188-190. DOI: 10.1016/j.jmmm.2007.02.085.

[12] Dutta, G.; Waghmare, U. V., Enhanced dielectric response in ZrO_2 with Th substitution: A first-principles study. *Solid State Commun.* **2008**, *146* (11-12), 495-497. DOI: 10.1016/j.ssc.2008.03.032.

[13] Ugwuoke, C. O.; Ezugwu, S.; Mammah, S. L.; Ekwealor, A. B. C.; Suguyima, M.; Ezema, F. I., Structural, optical and magnetic properties of Cu-doped ZrO_2 films synthesized by electrodeposition method. *Ceram. Int.* **2022**, *48*, 4686-4692. DOI: 10.1016/j.ceramint.2021.11.004.

[14] Pawar, K. S.; Baviskar, P. K.; Inamuddin, A. B.; Salunke-Gawali, S.; Pathan, H. M., Layer-by-layer deposition of TiO_2-ZrO_2 electrode sensitized with Pandan leaves: natural dye-sensitized solar cell. *Mater Renew Sustain Energy* **2019**, *8*, 1-9. DOI: 10.1007/s40243-019-0148-x.

[15] Sani, E.; Mercatelli, L.; Sans, J. L.; Sciti, D., Optical properties of black and white ZrO_2 for solar receiver applications. *Sol. Energy Mater. Sol. Cells* **2015**, *140*, 477-482. DOI: 10.1016/j.solmat.2015.02.007.

[16] Venkatesan, M.; Fitzgerald, C. B.; Coey, A. J., Unexpected magnetism in a dielectric oxide. *Nature* **2004**, *430* (7000), 630-630. DOI: 10.1038/430630a.

[17] Ostanin, S.; Ernst, A.; Sandratskii, L. M.; Bruno, P.; Däne, M.; Hughes, I. D.; Staunton J. B.; Hergert W.; Mertig I.; Kudrnovský, J., Mn-stabilized zirconia: From imitation diamonds to a new potential high-T C ferromagnetic spintronics material. *Phys. Rev. Lett.*

2007, *98* (1), 016101. DOI: 10.1103/PhysRevLett.98.016101.

[18] Zhang, Y. F.; Ren, H.; Hou, Z. T., First-principles calculations of electronic and optical properties of C-doped and F, C-codoped cubic ZrO_2. *J. Alloys Compd.* **2014**, *617*, 86-92. DOI: 10.1016/j.jallcom.2014.07.215.

[19] Pan, Y.; Pu, D.; Liu, G.; Wang, P., Influence of alloying elements on the structural stability, elastic, hardness and thermodynamic properties of Mo_5SiB_2 from first-principles calculations. *Ceram. Int.* **2020**, *46* (10), 16605-16611. DOI: 10.1016/j.ceramint.2020.03.233.

[20] Pan, Y.; Lin, Y.; Liu, G.; Zhang, J., Influence of transition metal on the mechanical and thermodynamic properties of IrAl thermal barrier coating. *Vacuum* **2020**, *174*, 109203. DOI: 10.1016/j.vacuum.2020.109203.

[21] Ijeh, R. O.; Nwanya, A. C.; Nkele, A. C.; Madiba, I. G.; Bashir, A. K. H.; Ekwealor, A. B. C.; Osuji, R.U.; Maaza, M.; Ezema, F., Optical, electrical and magnetic properties of copper doped electrodeposited MoO3 thin films. *Ceram. Int.* **2020**, *46* (8), 10820-10828. DOI: 10.1016/j.ceramint.2020.01.093.

[22] Scotti, N.; Bossola, F.; Zaccheria, F.; Ravasio, N., Copper-zirconia catalysts: Powerful multifunctional catalytic tools to approach sustainable processes. *Catalysts* **2020**, *10* (2), 168. DOI: 10.3390/catal10020168.

[23] Hussain, F.; Imran, M.; Khalil, R. A.; Sattar, M. A.; Niaz, N. A.; Rana, A. M.; Kim, S., A first-principles study of Cu and Al doping in ZrO_2 for RRAM device applications. *Vacuum* **2019**, *168*, 108842. DOI: 10.1016/j.vacuum.2019.108842.

[24] Pan, Y.; Zhang, J., Influence of noble metals on the electronic and optical properties of the monoclinic ZrO_2: a first-principles study. *Vacuum* **2021**, *187*, 110112. DOI: 10.1016/j.vacuum.2021.110112.

[25] Wang, H.; Lin, N.; Xu, R.; Yu, Y.; Zhao, X., First principles studies of electronic, mechanical and optical properties of Cr-doped cubic ZrO_2. *Chem. Phys.* **2020**, *539*, 110972. DOI: 10.1016/j.chemphys.2020.110972.

[26] Chouhan, L.; Bouzerar, G.; Srivastava, S. K., d0 Ferromagnetism in Ag-doped monoclinic ZrO_2 compounds. *Vacuum* **2020**, *182*, 109716. DOI: 10.1016/j.vacuum.2020.109716.

[27] Zhang, M.; Zhang, J.; Zhou, Z.; Chen, S.; Zhang, T.; Song, F.; Tsubaki, N.; Tan, Y.; Han, Y., Effects of the surface adsorbed oxygen species tuned by rare-earth metal doping on dry reforming of methane over Ni/ZrO_2 catalyst. *Appl. Catal. B* **2020**, *264*, 118522. DOI: 10.1016/j.apcatb.2019.118522.

[28] Zhang, Y. F.; Ren, H.; Hou, Z. T., First-principles calculations of electronic and optical properties of C-doped and F, C-codoped cubic ZrO_2. *J. Alloys Compd.* **2014**, *617*, 86-92. DOI: 10.1016/j.jallcom.2014.07.215

[29] Su, Q.; Zhang, Y.; Li, G.; Geng, Y.; Zheng, H.; Chen, Z.; Peng, P., Doped effect of Gd and Y elements on corrosion resistance of ZrO_2 in CMAS melt: First-principles and experimental study. *J. Eur. Ceram. Soc.* **2021**, *41* (15), 7893-7901. DOI: 10.1016/j.jeurceramsoc.2021.09.002.

[30] Ijeh, R. O.; Ugwuoke, C. O.; Ugwu, E. B.; Aisida, S. O.; Ezema, F. I., Structural, optical and magnetic properties of Cu-doped ZrO_2 films synthesized by electrodeposition method. *Ceram. Int.* **2022**, *48* (4), 4686-4692. DOI: 10.1016/j.ceramint.2021.11.004.

[31] Kumari, S.; Sharma, E.; Verma, J.; Dalal, J.; Kumar, A., Structural and photoluminescence properties of Dy-doped nanocrystalline ZrO_2 for optoelectronics application. *Ceram. Int.* **2023**, *49* (12), 20185-20192. DOI: 10.1016/j.ceramint.2021.11.004.

[32] Idrissi, S.; Ziti, S.; Labrim, H.; Bahmad, L., Sulfur doping effect on the electronic properties of zirconium dioxide ZrO_2. J. Mater. *Sci. Eng. B* **2021**, *270*, 115200. DOI: 10.1016/j.mseb.2021.115200.

[33] Saidi, F.; Mokhdar, S.; Dergal, M.; Mahmoudi, A.; Kallekh, A.; Abd El-Gawad, H. H., *Ab initio* study of the structural, electronic, magnetic, mechanical, optical, and dynamical properties of the rare-earth dihydrides MH2 (M = Yb, Sc, Eu, Y, Lu and Gd). *Vacuum* **2023**, *212*, 112011. DOI: 10.1016/j.vacuum.2023.112011.

[34] Saidi, F.; Mahmoudi, A.; Laidi, K.; Hidouri, T.; Nasr, S., Structural, electronic and optical properties of M-doped anatase TiO_2 (M = Fe or Au): a first principle investigation. *Comput. Condens. Matter* **2021**, *28*, 00576. DOI: 10.1016/j.cocom.2021.e00576.

[35] Kresse, G.; Furthmüller, J., Efficiency of *ab-initio* total energy calculations for metals and semiconductors using a plane-wave basis set. *Comput. Mater. Sci*. **1996**,

6 (1), 15-50. DOI: 10.1016/0927-0256(96)00008-0.

[36] Perdew, J. P.; Burke K.; Ernzerhof, M., Generalized gradient approximation made simple, *Phys. Rev. Lett.* **1996**, *77*, 3865. DOI: 10.1103/PhysRevLett.77.3865.

[37] Tran, F.; Blaha, P., Accurate band gaps of semiconductors and insulators with a semilocal exchange-correlation potential. *Phys. Rev. Lett.* **2009**, *102* (22), 226401. DOI: 10.1103/ PhysRevLett.102.226401.

[38] Sekkal, A.; Saidi, F.; Benzair, A.; Sahlaoui, M.; Esling, C.; Raulot, J. M., Structural and Physical Properties of DyCu, NdAg, LaCd, YIn, ErCu, ErAg, and ErAu Rare-Earth Intermetallic Compounds: *Ab initio* Investigations Analyzed by Data Mining Technique. *Phys. Solid State* **2020**, *62*, 2305-2317. DOI: 10.1134/ S1063783420120240.

[39] Murnaghan; F. D., The compressibility of media under extreme pressures. *Proc. Natl. Acad. Sci.* **1944**, *30* (9), 244-247. DOI: 10.1073/pnas.30.9.244.

[40] Bondars, B.; Heidemane, G.; Grabis, J.; Laschke, K.; Boysen, H.; Schneider, J.; Frey, F., Powder diffraction investigations of plasma sprayed zirconia. *J. Mater. Sci.* **1995**, *30*, 1621-1625. DOI: 10.1007/BF00375275.

[41] Houssa, M.; Afanas'ev, V. V.; Stesmans, A.; Heyns, M. M., Variation in the fixed charge density of SiOx/ZrO_2 gate dielectric stacks during postdeposition oxidation. *Appl. Phys. Lett.* **2000**, *77* (12), 1885-1887. DOI: 10.1063/1.1310635.

[42] Jomard, G.; Petit, T.; Pasturel, A.; Magaud, L.; Kresse, G.; Hafner, J., First-principles calculations to describe zirconia pseudopolymorphs. *Phys. Rev. B* **1999**, *59* (6), 4044. DOI: 10.1103/PhysRevB.59.4044.

[43] Seema, K.; Kumar, R., Effect of Dopant Concentration on Electronic and Magnetic Properties of Transition Metal-Doped ZrO_2. *J. Supercond. Novel Magn*. **2015**, *28*, 2735-2742. DOI: 10.1007/s10948-015-3086-6.

[44] Shen, T.; Hu, C.; Yang, W. L.; Liu, H. C.; Wei, X. L., Theoretical investigation of magnetic, electronic and optical properties of orthorhombic $YFeO_3$: A first-principle study. Mater. Sci. Semicond. *Process.* **2015**, *34*, 114-120. DOI: 10.1016/j.mssp.2015.02.015.

[45] Lucarini, V.; Peiponen, K. E.; Saarinen, J. J.; Vartiainen, E. M., Kramers-Kronig relations in optical materials research. *Springer Ser. Opt. Sci*. **2005**, *110*.

[46] Sathyaseelan, B.; Manikandan, E.; Baskaran, I.; Senthilnathan, K.; Sivakumar, K.; Moodley, M. K.; Ladchumananandasivam, R.; Maaza, M., Studies on structural and optical properties of ZrO_2 nanopowder for opto-electronic applications. *J. Alloys Compd*. **2017**, *694*, 556-559. DOI: 10.1016/j.jallcom.2016.10.002.

[47] Maji, P.; Choudhary, R. B.; Majhi, M., Structural, optical and dielectric properties of ZrO_2 reinforced polymeric nanocomposite films of polymethyl-methacrylate (PMMA). *Optik* **2016**, *127*, 4848-4853. DOI: 10.1016/j.ijleo.2016.02.025.